ACS Sustainable Chemistry & Engineering

pubs.acs.org/journal/ascecg

Research Article

Repurposing of Blackcurrant Pomace via Microwave-Assisted Hydrothermal Fractionation into pH-Sensitive Films

Natthamon Inthalaeng, Thomas Iain James Dugmore, and Avtar Singh Matharu*

Cite This: *ACS Sustainable Chem. Eng.* 2025, 13, 13988−14002

Read Online

ACCESS | Metrics & More | Article Recommendations | Supporting Information

ABSTRACT: The valorization of unavoidable food waste and repurposing through the adoption of circular, zero-waste principles is an important driver to combat global grand challenges of food security, responsible consumption and production, and, ultimately, climate change. Herein, the microwave-assisted hydrothermal valorization of blackcurrant pomace into anthocyanin (ACN), blackcurrant pectin (BCP), and defibrillated cellulose (DFC) fractions and their repurposing into pH-sensitive sodium alginate (NaAlg) films is reported. The inclusion of BCP, DFC, and ACN fractions into NaAlg matrices positively affected the antioxidant activity. The inclusion of BCP primarily influenced the mechanical properties and hydrophilicity of films. NaAlg−BCP films were able to detect ammonia, with NaAlg−BCP50 showing the most distinct color change. Moreover, NaAlg−BCP50 showed reversible color changes upon sequential exposure to NH_3 and CH_3COOH. Differential scanning calorimetry (DSC) showed that the films are suitable for relatively high-temperature food applications (up to 187 °C). In addition, the films demonstrated antifogging properties due to their high water vapor permeability (WVP), supporting their use in packaging for highly perishable produce. This work demonstrates the potential for reducing unavoidable food waste and repurposing it into intelligent food spoilage indicator films.

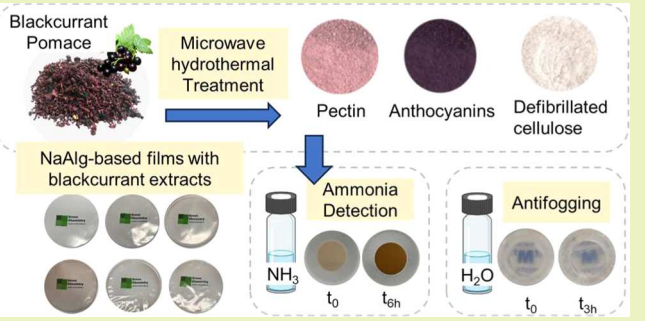

KEYWORDS: *blackcurrant pomace, microwave hydrothermal treatment, biomaterials, anthocyanins, pectins, pH-responsive films*

1. INTRODUCTION

The global population is estimated to reach approximately 10.3 billion by 2080,[1] which will directly impact food security, food scarcity, and food supply chains. Ironically, in 2022, 1.05 billion tons of food waste were generated.[2] In line with the United Nations Sustainable Development Goals (SDGs), particularly SDG 12: Ensure sustainable consumption and production patterns, these issues must be addressed through a food security lens that focuses on circular economy concepts, doing more with less, reusing and repurposing byproducts, and adopting zero-waste strategies throughout the food supply chain.

Unavoidable food supply chain byproducts, such as agro-industrial waste, are valuable sources of bioactive compounds and structural biopolymers.[3,4] Blackcurrant pomace , a major product after juice processing, which particularly consists of anthocyanins (ACNs), blackcurrant pectin (BCP), and cellulose,[5,6] presents a significant opportunity for value-added applications in sustainable material development.[7,8] The demand for biodegradable and functional packaging materials is growing, leading to an upsurge in research focused on converting such biomass into active films with tailored properties.[9,10]

Current research has largely focused on the separation of natural colorants and biopolymers from various agricultural sources, followed by recombination into biobased packaging.[9−11] However, the residual biomass remaining after extraction is overlooked, although it can be potentially converted to value-added products. Moreover, conventional extraction methods for biopolymers such as pectin and cellulose typically involve harsh chemicals, which can pose environmental and sustainability concerns.[5]

Microwave hydrothermal extraction has been reported as an environmentally friendly and efficient method for the isolation of pectin and defibrillated cellulose (DFC) from various biomass sources.[12−14] Compared with conventional techniques, it offers better energy efficiency, shorter processing times, and reduced chemical usage. In addition to its effectiveness for biopolymer recovery, microwave-assisted extraction has also shown promising results in enhancing the extraction of bioactive compounds, including phenolics and ACNs, due to improved cell wall disruption and solvent penetration.[15,16]

Received: May 29, 2025
Revised: August 11, 2025
Accepted: August 11, 2025
Published: August 18, 2025

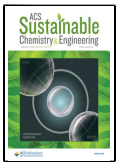

ACNs, pH-responsive pigments,[22−25] have been widely studied for their application in pH-sensitive intelligent films, offering added antioxidant and antibacterial benefits.[17,18] Incorporating ACNs into films can lead to a color change at different pH levels, making them effective indicators for monitoring food spoilage, such as in fish, shrimp, pork, and milk.[17,19−21] Additionally, combining ACN extracts with other biopolymers, such as chitosan, carrageenan, and cellulose, is both biodegradable and safe for handling and applicable in the food industry.[9,18,20]

Several techniques, including biopolymer blending,[9,22] cross-linking,[18,22,23] and reinforcement adding,[11,24] have been proposed for improving film properties. For instance, Gohil et al. and Nei et al. demonstrated the synergistic effect of sodium alginate (NaAlg)−pectin blending under calcium chloride or zinc chloride cross-links, where the carboxyl groups of NaAlg and pectin interact with calcium ions or zinc ions, creating the "egg box" model. The unique physical cross-linking of the amorphous molecular structure of the "egg box" resembles the structure of the synthetic semicrystalline polymers, called "fringed-micellar", resulting in improved mechanical properties.[22,25] Rezvanian et al. further investigated the optimal condition of cross-linking of NaAlg−pectin hydrogel films, in which 0.5 wt% calcium chloride positively affected mechanical properties.[26] Moreover, Lei et al. introduced cellulose nanocrystals as a reinforcement agent to NaAlg−pectin smart films incorporating ACNs from red cabbage. The optimally prepared film demonstrated a pH-indicating material that can be used for shrimp freshness monitoring with reduced water solubility and enhanced mechanical strength.[19] In this study, blackcurrant pomace is explored as a single source of ACNs as a pH-responsive agent, BCP, as a biopolymeric matrix, and DFC, as a filler/reinforcement agent, in the production of pH-sensitive sodium alginate films (Figure S1). Importantly, all three components are simultaneously extracted using microwave hydrothermal treatment, demonstrating a more environmentally friendly and energy-efficient alternative to conventional extraction methods.

2. RESULTS AND DISCUSSION

2.1. Characterization of Blackcurrant Pomace ACN-Rich Extracts. Blackcurrant ACNs from ethanol−water (ETW) and microwave extracts were identified via high-performance liquid chromatography−ultraviolet−mass spectrometry (HPLC−UV−MS).[27] The chromatograms of blackcurrant extracts monitored at 520 nm and their analysis are depicted in Figure S2 and summarized in Table S1. Delphinidin-3-glucoside (D3G), delphinidin-3-rutinoside (D3R), cyanidin-3-glucoside (C3G), and cyanidin-3-rutinoside (C3R) were identified as the major ACNs extracted, which correlate well with the literature.[6,28,29] The ETW extract of blackcurrant pomace was found to have the highest total anthocyanin content (TAC) (15.32 mg C3G/g) among all extracts (Table 1). Meanwhile, the TAC of microwave extracts decreased from 7.22 mg C3G/g to not detected (n.d.) as the microwave extraction temperature increased from 100 to 160 °C. In contrast, the total phenolic content (TPC) varied from 28.30 to 195.54 mg GA/g with increasing microwave temperatures, indicating the higher efficiency of microwaves for phenolic extraction. Furthermore, microwave extraction at high temperatures causes thermal degradation of ACNs into phenolics, especially cyanidin, which thermally degrades into protocatechuic acid, 4-hydroxybenzoic acid, and phloroglucinaldehyde.[30] Moreover, phloroglucinaldehyde and gallic acid can be obtained from the thermal degradation of delphinidin.[31] The antioxidant activity of the blackcurrant pomace extracts (Table 1) was determined by the 2,2-diphenyl-1-picrylhydrazyl (DPPH) assay and expressed as DPPH inhibition (%). The DPPH inhibition of blackcurrant pomace extracts varied from 66 to 86%, with the lowest value found in the ETW extract.

Table 1. TPC, TAC, and Antioxidant Activity[a]

sample	TPC (mg GA/g)	TAC (mg C3G/g)	DPPH inhibition (%)
ETW	28.30 ± 6.94[a]	15.32 ± 2.15[a]	65.94 ± 0.12[d]
MW100	94.31 ± 0.34[b]	7.22 ± 0.66[b]	85.29 ± 0.05[b]
MW120	163.82 ± 3.92[c]	4.21 ± 0.53[c]	85.03 ± 0.43[b]
MW140	195.54 ± 4.07[d]	0.78 ± 0.04[d]	86.27 ± 0.54[a]
MW160	131.07 ± 3.01[e]	n.d.	68.75 ± 0.29[c]

[a]Values are presented as mean ± SD (n = 3). Lowercase letters indicate the significant differences (p < 0.05).

These results are in good accordance with the literature, showing that microwave-assisted extraction of blackcurrant helps improve phenolic content compared to conventional hot solvent extraction, in which the TPC increased from 31.25 (conventional extraction) to 41.77 mg GA/g (deionized water, microwave, 780 W, 60 min)[16] and from 26.32 (conventional extraction) to 40.19 mg/g (microwave, 600W, 10 min).[32] The TPC yield significantly increases to 58.60 mg/g when microwave-assisted aqueous two-phase extraction was applied.[32]

Based on our findings, microwave-assisted hydrothermal extraction (MW) at 100 °C (MW100) is recommended for ACN extraction, which can yield high TAC without requiring any additional mineral acid or organic solvent. The highest TAC value of microwave-assisted hydrothermal extracts was 7.22 mg of C3G/g (Table 1). Although the obtained TAC value is lower than that of blackcurrant extract obtained from microwave-assisted acid extraction (20.4 mg C3G/g at 700W, pH 2),[15] it is higher than that of the TAC of microwave-assisted ethanolic extraction (104.09 mg C3G/100g or 1.04 mg C3G/g, 30% ethanol).[33]

The optical properties of the blackcurrant pomace extracts across the full pH range were investigated by using ultraviolet−visible (UV−vis) spectroscopy (Figure 1). The shift in the maximum absorption peak is primarily due to the color change of blackcurrant pomace extracts with pH, which is influenced by the ionic nature of the CAN, which can undergo structural transitions in response to changes in pH: from red flavylium cation (pH < 3) to colorless carbinol pseudo base, by hydration (pH 4−5), to blue quinonoidal base (pH 6−9) and finally to yellow chalcones (pH > 10).[21,34,35] As the pH of the solution increases from 1 to 11, the maximum absorption peak undergoes a notable hypsochromic (blue) shift from approximately 495 nm to below 400 nm, accompanied by a color change from red to yellow. The MW100 extract was chosen for further application in pH-responsive film fabrication because it responded well to both acid and base. In contrast, all other microwave extracts had less ability to respond to an acidic pH.

2.2. Characterization of NaAlg and NaAlg−BCP Films. The appearance and microstructures of NaAlg and NaAlg−BCP films on the surface and cross section were examined using scanning electron microscopy (SEM) (Figure 2). All of the NaAlg and NaAlg−BCP films are transparent (Figure 2A). The NaAlg film exhibited an amorphous-like texture, illustrated

https://doi.org/10.1021/acssuschemeng.5c05240
ACS Sustainable Chem. Eng. 2025, 13, 13988−14002

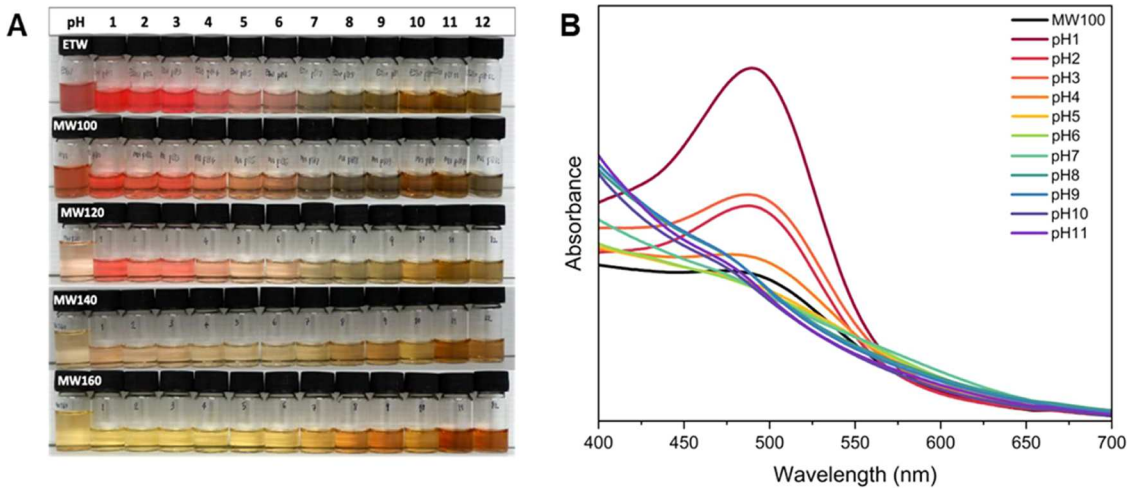

Figure 1. (A) Visual appearance of aqueous solutions of extracts from pH 1 to 12. (B) UV−vis spectra of MW100 extract aqueous solutions from pH 1 to 11.

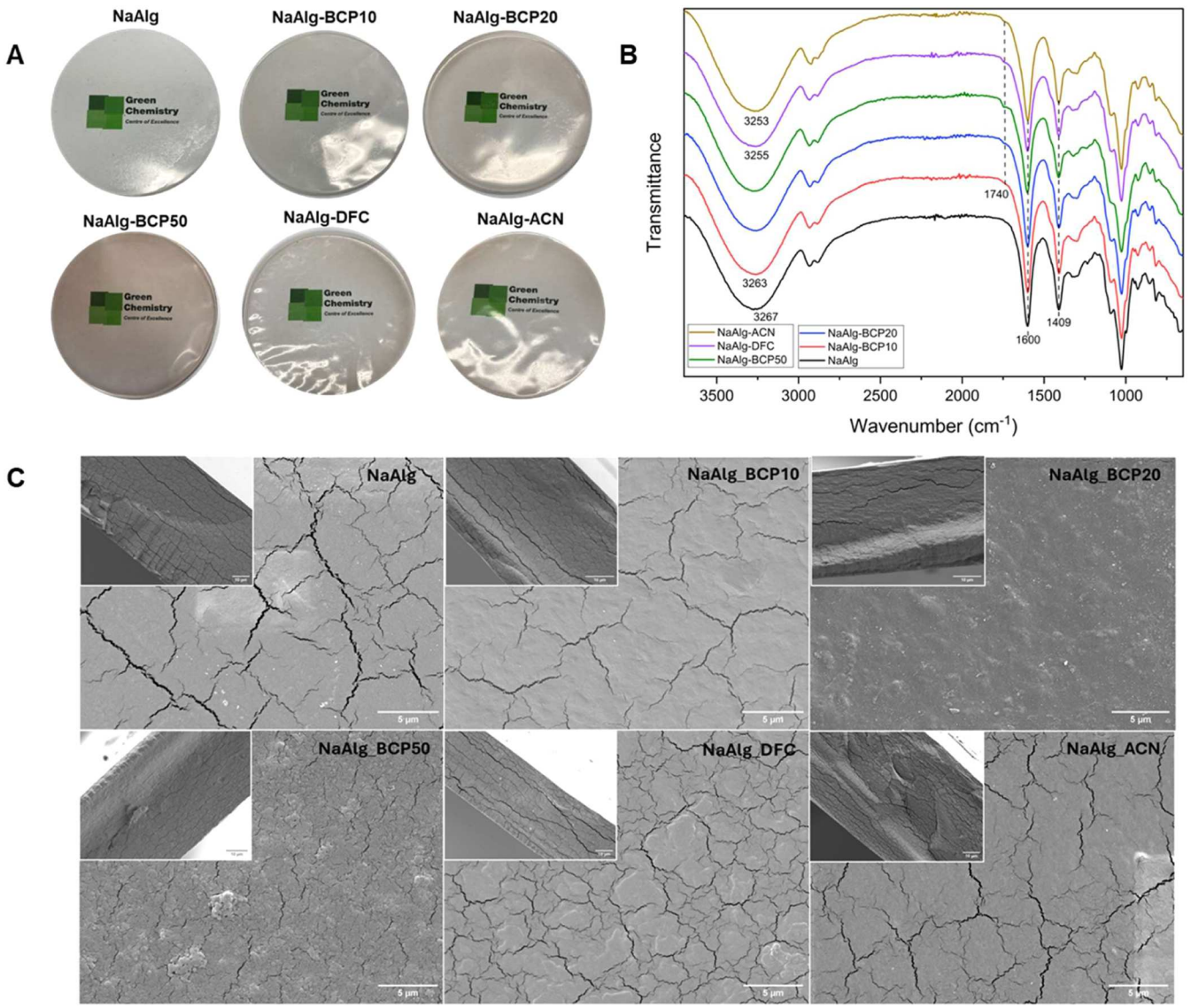

Figure 2. (A) Visual appearance, (B) ATR-IR spectra, and (C) SEM images (insets show cross sections (4000×)) of NaAlg−BCP films.

https://doi.org/10.1021/acssuschemeng.5c05240
ACS Sustainable Chem. Eng. 2025, 13, 13988−14002

by smooth surfaces without pores or holes from top to bottom. However, some cracking was observed, likely attributable to the soft nature of the polymer films. The cross-sectional fractures indicate good homogeneity within the films. The interactions between BCP, NaAlg, and the Ca^{2+} ions likely contributed to forming a more stable and uniform network (Figure 2C). Incorporation of DFC or ACN into the NaAlg−BCP20 film altered its microstructure, giving the surface a rougher and less homogeneous appearance. The addition of DFC or ACN appeared to disrupt the polymer network, resulting in a less structured film and consequently reducing its tensile strength (see later). Similarly, cracking has been observed in the literature when ACNs from rose and blackcurrant were added to NaAlg/apricot peel pectin films and konjac glucomannan/carboxymethyl cellulose films.[25,26]

Attenuated total reflectance infrared (ATR-IR) analysis was used to confirm the functional groups present in the films (Figure 2B). All films exhibited the main characteristic absorption bands associated with the structure of NaAlg at around 3267 (O−H str.), 2920 (C−H str.), 1605 (COO− str.), and 1409 cm^{-1} (C−C or C−O str.).[19,36] After BCP was added, a new band was observed at 1740 cm^{-1}, attributable to the methyl ester of galacturonic acid within pectin or possibly the product of esterification of pectin and glycerol. No new significant absorbance bands were observed after adding either DFC or ACN. The O−H stretching band in NaAlg−BCP20 at 3263 cm^{-1} shifted to 3255 and 3253 cm^{-1} for NaAlg−DFC and NaAlg−ACN, respectively. This change may be due to the incorporation of NaAlg−BCP and DFC or NaAlg−BCP and ACN through hydrogen bonding.[19,37,38]

2.3. Mechanical Properties of Films. The tensile strength of NaAlg−BCP films ranged from 2.14 to 5.15 MPa, while the tensile strain at break ranged between 1.86 and 2.98 mm/mm (Table 2). It was observed that the NaAlg−BCP50 film exhibited the highest tensile strength among all of the NaAlg−BCP films. However, there was no significant difference between the other NaAlg−BCP films. This is possibly due to the synergistic effect of NaAlg−pectin blending,[25] where the carboxyl groups of NaAlg and pectin interact with calcium ions, creating the "egg box" model. The unique physical cross-linking of the amorphous molecular structure of the "egg box" resembles the structure of the synthetic semicrystalline polymers known as "fringed-Micellar"[25] and may have contributed to the increased strength of the films. This aligns with results from the literature, where a similar highest tensile strength trend was found at around 40% pectin content.[25] Moreover, the higher tensile strength of the NaAlg film when adding BCP may also be due to hydrogen bonding between molecular polymer chains[39] and the chemical cross-linking between glycerol and nonesterified pectin structures.[40] However, the interaction that improves the tensile strength property of the films leads to a densely packed structure, resulting in reduced tensile strain at break of the NaAlg−BCP films with increased BCP content.

Table 2. Mechanical Properties of NaAlg−BCP Films[a]

sample	tensile stress (MPa)	tensile strain at break (ε, mm/mm)
NaAlg	2.90 ± 1.22^{a}	2.59 ± 0.40^{bc}
NaAlg−BCP10	2.72 ± 0.40^{a}	2.98 ± 0.36^{c}
NaAlg−BCP20	2.88 ± 1.73^{a}	2.22 ± 0.42^{ab}
NaAlg−BCP50	5.15 ± 1.60^{b}	1.86 ± 0.25^{a}
NaAlg−DFC	2.14 ± 0.41^{a}	1.88 ± 0.21^{a}
NaAlg-CAN	2.26 ± 0.37^{a}	2.37 ± 0.26^{ab}

[a]Values are presented as mean ± SD (n = 3−6). Lowercase letters indicate the significant differences ($p < 0.05$).

The addition of DFC into the NaAlg−BCP20 film resulted in reduced tensile strength and tensile strain at break. This phenomenon may be attributed to the residual insoluble lignin present in DFC, which was found to be up to 20% in our previous study.[7] The presence of insoluble lignin could interfere with intramolecular interactions between NaAlg/BCP and DFC, potentially leading to a discontinuous polymer network and the formation of defect zones, thereby limiting reinforcement within the film matrix. Unlike DFC, the addition of ACN decreased the tensile strength of the NaAlg−BCP film; however, a slight increase in the tensile strain at break was observed. This could be attributed to the plasticizing effect of ACN. As small polyphenolic molecules, ACNs can act as plasticizers by interacting with NaAlg/BCP polymer chains through hydrogen bonding. These interactions enhance chain mobility, leading to increased film flexibility.[41] However, the presence of ACN may also disrupt intramolecular interactions within the polymer matrix, thereby weakening the overall film structure.[41] This finding was consistent with previous studies, which suggested that polyphenols can inhibit the chain interaction in the film structure, thereby reducing the tensile strength.[20,48,9,22] In addition, the tensile strength of the NaAlg and NaAlg−BCP films is significantly lower than that of commercial packaging, ranging from around 15 to 70 MPa.[42] This limitation may be influenced by the structural characteristics of NaAlg, which consists of different polymer block types, including homopolymeric blocks (MM or GG) and alternating blocks (MG or GM). Among these, GG blocks have a stronger affinity for binding with Ca^{2+} ions, which can enhance cross-linking and improve mechanical strength.[43] Therefore, optimizing the ratio of mannuronic acid (M) to guluronic acid (G) monomers and selecting NaAlg with a higher content of GG blocks could be promising strategies to enhance the tensile strength of NaAlg−BCP films. Moreover, the incorporation of biobased acid cross-linkers may offer additional mechanical reinforcement. For instance, Singh et al. demonstrated that NaAlg/pectin films cross-linked with citric acid and tartaric acid through covalent bonding exhibited tensile strength values of up to 18 MPa.[44]

2.4. Rheological Properties of NaAlg−BCP Film-Forming Solutions. Viscosity significantly influences film properties such as thickness, spread ability, mechanical properties and homogeneity of films.[45,46] All rheology curves (Figure S3) exhibited shear thinning behavior in which increasing shear rate decreases shear viscosity. This behavior indicates the deformation of the entanglement structure and the reduction of intermolecular forces between pectin and NaAlg with increasing shear rate. The weakening of intermolecular forces with increasing shear rate is consistent with the berry pectin gel and NaAlg solution.[47,48] Compared with the NaAlg solution alone, solutions with higher concentrations of BCP showed lower shear viscosity (Figure S3-A), suggesting that NaAlg primarily dominates the viscosity of NaAlg−BCP solutions. The shear viscosity upon the addition of glycerol as a plasticizer (Figure S3−B) was slightly lower than that without glycerol in the NaAlg−BCP solutions. Glycerol molecules are able to occupy intermolecular spaces between polymer chains, weakening the ordered polymer network.[45] As expected, the addition of a calcium cross-linker

https://doi.org/10.1021/acssuschemeng.5c05240
ACS Sustainable Chem. Eng. 2025, 13, 13988−14002

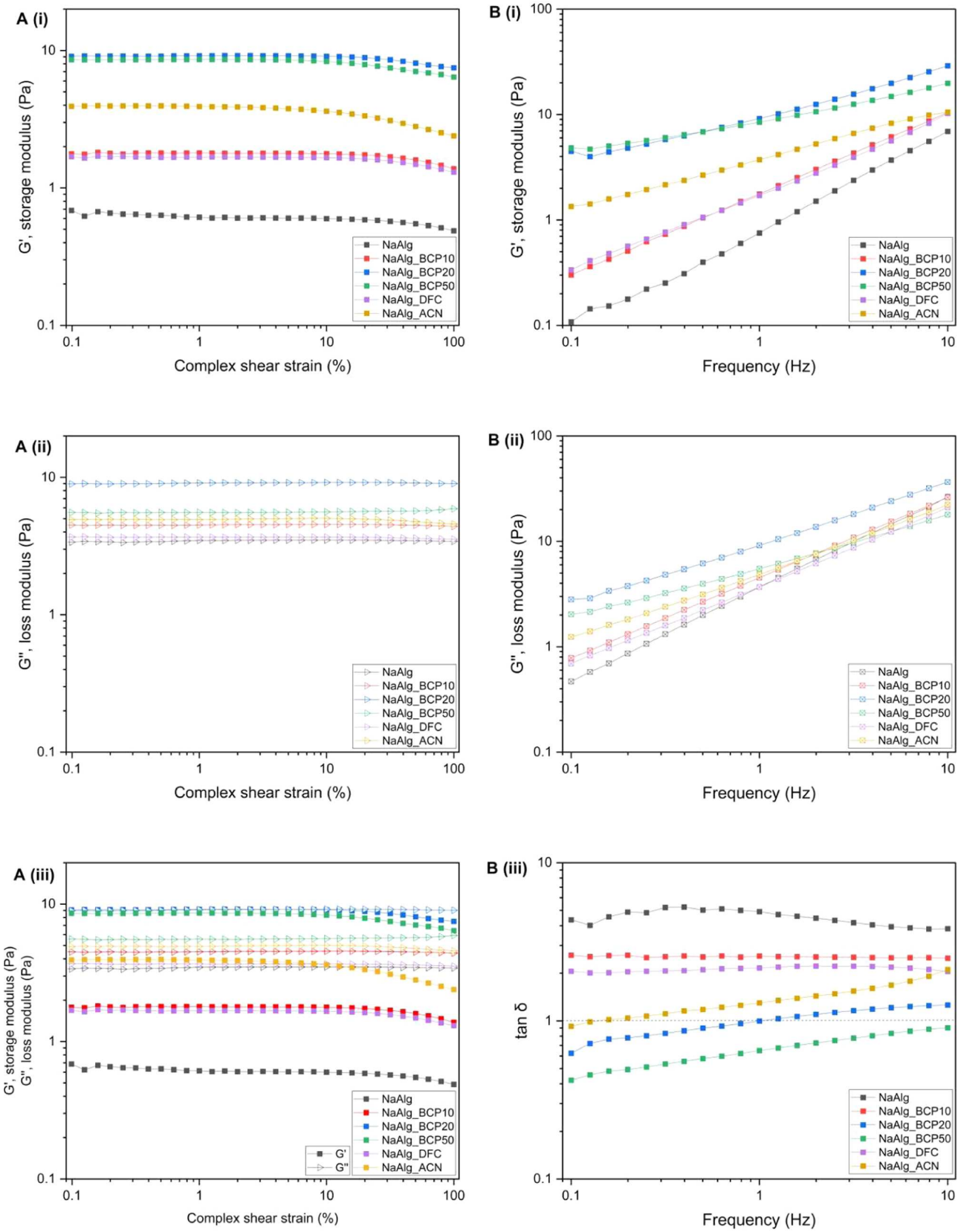

Figure 3. Rheological properties of NaAlg−BCP film-forming solutions. (A) Amplitude sweep curves showing (i) storage modulus (G'), (ii) loss modulus (G''), and (iii) comparison of storage (G') and loss (G'') moduli. (B) Frequency sweep curves showing (i) storage modulus (G'), (ii) loss modulus (G''), and (iii) loss tangent ($\tan \delta$).

increased the shear viscosity of NaAlg−BCP solutions (Figure S3−C), confirming the formation of "egg box" structures and an interlinked networks involving NaAlg, BCP, and Ca^{2+} ions. The highest shear viscosity among the NaAlg−BCP film-

https://doi.org/10.1021/acssuschemeng.5c05240
ACS Sustainable Chem. Eng. 2025, 13, 13988−14002

forming solutions containing Ca^{2+} ions was observed in the NaAlg−BCP20 formulation, followed by NaAlg−BCP50, NaAlg−BCP10, NaAlg, NaAlg−ACN, and NaAlg−DFC. However, no significant differences in shear viscosity were found among NaAlg−BCP10, NaAlg, NaAlg−ACN, and NaAlg−DFC. The shear viscosity results generally correlated well with the tensile strength of the corresponding NaAlg−BCP films. Specifically, NaAlg−BCP10, NaAlg, NaAlg−ACN, and NaAlg−DFC films exhibited no significant differences in tensile strength, while NaAlg−BCP50 showed a relatively higher value.

The amplitude sweep test of the NaAlg−BCP film-forming solutions containing glycerol and $CaCl_2$ (Figure 3A) was conducted to evaluate the linear viscoelastic region (LVR) and rheological stability of the viscoelastic solid/liquid. All curves showed the LVR within a strain of 1%, and the crossover point or yield point was not observed in the range of study (strain of 0.1−100%). The NaAlg solution predominantly displayed viscoelastic liquid behavior, and a higher value of loss modulus (G'') over storage modulus (G') was observed.

The frequency sweep test was conducted to observe the change in the stability and microstructure of the film-forming solution during storage or transportation.[10,45] The frequency sweep test of the NaAlg−BCP film-forming solutions containing glycerol and $CaCl_2$ (Figure 3B) was conducted within the LVR, as determined earlier by the amplitude sweep test. The G' and G'' of the NaAlg−BCP film-forming solutions increased with increasing frequency (Figure 3B(i and ii)). The tan δ, the ratio of loss modulus (G'') to storage modulus (G'), reflects the balance between the viscous and elastic behavior.[49] The tan δ (Figure 3B(iii)) of the NaAlg solution was greater than 1, indicating liquidlike behavior ($G'' \gg G'$). The tan δ values of NaAlg−BCP solutions decreased with increasing BCP content and the addition of DFC or ACN, reflecting a transition from a more liquidlike ($G'' > G'$) to a more solidlike ($G' > G''$) matrix. This shift is primarily attributed to the cross-linking of the higher content of low-DE BCP facilitated by Ca^{2+} ions, where enhanced entanglement contributes to an increase in solidlike behavior.[46] However, the tan δ of NaAlg−BCP50 remained below 1 throughout the entire frequency sweep test, signifying consistently solidlike behavior within the range of study. It can be seen that the viscosity of NaAlg−BCP solutions incluiding glycerol and $CaCl_2$ increased with increasing BCP content (Figure S3−C), while tan δ decreased (Figure 3B(iii)), indicating that adding BCP can improve the elastic property of NaAlg solutions.

The creep recovery test evaluates the elasticity of materials.[50] NaAlg and NaAlg−BCP10 showed a small recovery and largely permanent deformation with the recovery values of 1.12 and 0.19%, respectively (Figure 4 and Table 3), indicating predominantly viscous behavior with negligible elasticity. As the BCP content increased, the recovery improved significantly, with NaAlg−BCP50 exhibiting the highest recovery (93.53%). This reflects a shift toward elastic (solidlike) behavior due to the enhanced network structure created by BCP, which allows the material to regain its original shape partially. For the NaAlg−BCP20 solution, the addition of DFC or ACN exhibited a reduction in recovery from 64.82 to 9.01% or 4.33%, respectively. This again confirms the decrease in network structure, which may be due to DFC or ACN interference.

According to the frequency sweep and creep recovery tests, increasing the BCP content in NaAlg films resulted in lower tan δ values and higher recovery rates, indicating enhanced elastic behavior in the film-forming solutions. However, this trend contrasts with the mechanical properties of the final films (Table 2), where a higher BCP content was associated with a decrease in tensile strain at break, suggesting reduced flexibility. This may be due to water loss during film drying, which leads to structural rearrangement and densification of the polymer network, resulting in different mechanical behaviors in the final films.

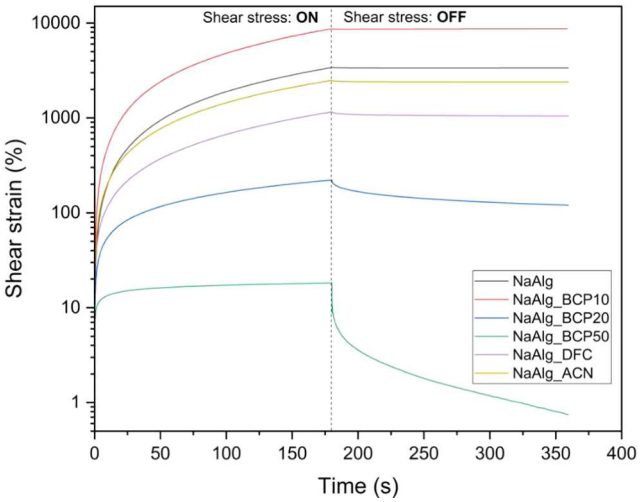

Figure 4. Strain (%) experienced by the NaAlg−BCP film-forming solutions when subjected to a creep recovery test at a constant shear of 0.5 Pa.

Table 3. Recovery (%) of the NaAlg−BCP Film-Forming Solutions[a]

samples	recovery (%) at a shear stress of 0.5 Pa
NaAlg	1.12 ± 0.23^{cd}
NaAlg−BCP10	0.19 ± 0.23^{d}
NaAlg−BCP20	64.82 ± 6.89^{b}
NaAlg−BCP50	93.53 ± 3.29^{a}
NaAlg−DFC	9.01 ± 1.13^{c}
NaAlg−ACN	4.33 ± 0.69^{cd}

[a]Values are presented as mean ± SD (n = 3). Lowercase letters indicate the significant differences ($p < 0.05$).

2.5. Physical Properties of Films. The control film (NaAlg) had a thickness of 0.074 mm and the highest moisture content among all of the films (Table 4). The addition of BCP resulted in no significant difference in thickness compared to the control film. This is in good accordance with previous literature, where no differences in thickness were observed between alginate and alginate−commercial low-methoxy pectin films.[36] The introduction of either DFC or ACN from blackcurrant pomace extracts into the NaAlg−BCP20 solution led to a gradual increase in the film thickness from 0.065 mm (NaAlg−BCP20) to 0.078 mm (NaAlg−DFC) or 0.077 mm (NaAlg−ACN). This increase in thickness is likely due to the higher dry matter content of DFC and ACN. A similar trend was observed when cellulose nanocrystals were added to NaAlg−pectin and NaAlg−pectin−red cabbage ACN films,[19] as well as when incorporating blackcurrant waste powder to chitosan or pectin films.[51]

The hydrophobicity or hydrophilicity of the surface of the films was determined by water contact angle measurements (Table 4 and Figure S4). The contact angle of the NaAlg film

https://doi.org/10.1021/acssuschemeng.5c05240
ACS Sustainable Chem. Eng. 2025, 13, 13988−14002

Table 4. Physical, Water Vapor Transmission, and Antioxidant Properties of NaAlg and NaAlg−BCP Films[a]

sample	thickness (mm)	moisture content (%)	water contact angle (deg) at 60 s	WVTR ($\times 10^{-3}$ g/s·m^2)	WVP ($\times 10^{-11}$ g/m·s·Pa)	DPPH inhibition (%)
NaAlg	0.074 ± 0.011^{ab}	27.75 ± 1.79^{a}	21.67 ± 1.79^{a}	4.35 ± 0.82^{b}	8.53 ± 0.63^{ab}	n.d.
NaAlg−BCP10	0.068 ± 0.008^{ab}	16.53 ± 1.31^{b}	30.71 ± 1.81^{b}	2.16 ± 0.48^{c}	5.54 ± 1.05^{a}	1.50 ± 0.16^{a}
NaAlg−BCP20	0.065 ± 0.010^{a}	14.94 ± 1.41^{b}	38.47 ± 0.75^{c}	3.12 ± 0.42^{bc}	5.74 ± 1.13^{a}	4.55 ± 0.07^{b}
NaAlg−BCP50	0.066 ± 0.009^{ab}	14.54 ± 1.17^{b}	47.02 ± 0.91^{d}	3.94 ± 0.32^{bc}	7.57 ± 0.52^{ab}	25.66 ± 0.11^{e}
NaAlg−DFC	0.078 ± 0.015^{c}	10.72 ± 0.94^{c}	39.06 ± 1.39^{c}	4.22 ± 0.88^{bc}	10.53 ± 2.16^{b}	9.17 ± 0.38^{c}
NaAlg−ACN	0.077 ± 0.012^{bc}	14.70 ± 1.17^{b}	37.98 ± 0.38^{c}	4.64 ± 1.15^{b}	11.21 ± 2.93^{b}	14.53 ± 0.11^{d}

[a]Values are presented as mean ± SD (n = 3−6). Lowercase letters indicate the significant differences (p < 0.05).

was 21.67° (60 s), and it increased with increasing BCP concentration. The NaAlg−BCP films showed contact angles higher than the NaAlg films, indicating a relatively more hydrophobic surface in the former. However, all contact angles of the NaAlg−BCP films were less than 90°, indicating that all of the films have hydrophilic surfaces.

2.6. Water Vapor Transmission Properties. The water vapor transmission rate (WVTR) and water vapor permeability (WVP) of NaAlg−BCP films reflect the moisture transfer property of the film. The WVTR was observed in a range of 2.16−4.64 × 10^{-3} g/s·m^2, while the WVP ranged from 5.54 to 11.21 × 10^{-11} g/m·s·Pa (Table 4). A similar trend was observed for both WVTR and WVP, in which the NaAlg film exhibited a higher value than NaAlg−BCP10, NaAlg−BCP20, and NaAlg−BCP50 films. This reduction can be attributed to the denser network formed between NaAlg and BCP through intramolecular interactions, resulting in lower WVTR and WVP values. However, the addition of DFC or ACN resulted in increased WVTR and WVP values compared to the NaAlg film, possibly due to the accumulation of DFC or ACN within the polymer network, which created greater free volume in the films. The increased free volume facilitated a higher rate of water vapor transmission, thereby enhancing the moisture permeability of films.[52,53]

The WVTR and WVP values of NaAlg−BCP films were lower than the previous findings, where NaAlg−$CaCl_2$ films exhibited higher WVTR values, ranging from 13.38 to 36.70 × 10^{-3} g/s·m^2,[54] and NaAlg−pectin−$ZnCl_2$ films showed WVP values between 23.9 and 51.3 × 10^{-11} g/m·s·Pa.[22] The relatively lower WVTR and WVP values of NaAlg−BCP films compared to those of NaAlg−$CaCl_2$ films and NaAlg−pectin−$ZnCl_2$ films may be due to the differences in measurement methods. This study employed the dry cup method, whereas the others used the wet cup method,[22,54] which typically yields higher permeability values.[55,56] However, the relatively high WVTR and WVP values of the NaAlg−BCP films, which are significant higher than the commercial low-density polyethylene films (a WVTR of 7.23 × 10^{-5} g/s·m^2 and a WVP of 8.46 × 10^{-16} g/m·s·Pa), suggest their potential to regulate water vapor transmission and reduce condensation, thereby providing antifogging functionality and helping to extend the shelf life of perishable products.[52]

2.7. Antifogging Properties. Since the NaAlg−BCP films possess a hydrophilic surface, as evidenced by water contact angles below 90° and high water vapor transmission properties, their antifogging behavior was further evaluated. The fogging test was visually assessed using NaAlg−BCP films, with a glass slide serving as the control. The results were scored and are summarized in Table 5 and Figure S5. At the initial point (t_0), all NaAlg−BCP films and the glass slide appeared completely transparent (score A). The control glass slide revealed a fogging surface (score B) within 5 min of water vapor exposure and developed small, discrete water droplets (score C) by 30 min of exposure. With prolonged exposure, an increase in the water droplet size was observed (scores D and E). In contrast, the NaAlg−BCP films maintained their transparency for up to 20 min under heating. By 30 min, slight crinkling on the film surface and a reduction in transparency was observed (scores A and B). Although the reduced transparency was observed, no fogging was observed on the NaAlg−BCP film surface. This condition remained stable up to 180 min of exposure to heated water vapor. The antifogging property of NaAlg−BCP films can be attributed to their hydrophilic nature, which enables rapid absorption of water vapor through hydrogen bonding.[52,57] In addition, the relatively high WVTR and WVP values of the films facilitate the transmission of water vapor through the film. As a result, no condensed water droplets were observed on the film surface. Therefore, the hydrophilic nature of the NaAlg−BCP films, combined with their high water vapor permeability, contributes to their effective antifogging performance.

Table 5. Antifogging Scores (A−E) of the Glass Slide and NaAlg−BCP Films over a 180 min Period

sample	test time (min)							
	t_0	t_5	t_{10}	t_{20}	t_{30}	t_{60}	t_{120}	t_{180}
glass slide (control)	A	B	B	B	C	D	E	E
NaAlg	A	A	A	A	A	A-B	A-B	A-B
NaAlg−BCP10	A	A	A	A	A-B	A-B	A-B	A-B
NaAlg−BCP20	A	A	A	A	A-B	A-B	A-B	A-B
NaAlg−BCP50	A	A	A	A	A-B	A-B	A-B	A-B
NaAlg−DFC	A	A	A	A	A-B	A-B	A-B	A-B
NaAlg−ACN	A	A	A	A	A-B	A-B	A-B	A-B

2.8. Antioxidant Properties of Films. The antioxidant activity of NaAlg−BCP films, represented by the percentage of DPPH inhibition, increased with an increase in the BCP content (Table 4). The higher DPPH inhibition of the NaAlg−BCP films may be attributed to the higher ACN-bound or remaining polyphenolics in BCP. Similar results were found in pectin extracted from lemon, pomelo, and pitaya peels.[58] The incorporation of either DFC or ACN into NaAlg−BCP20 films improved the antioxidant activity. This may be due to residual lignin in the DFC, the ACN in BC extract, or a combination of both factors.[20,59] This suggests that adding BCP to the NaAlg film improves both tensile properties and antioxidant activity. NaAlg−BCP50 demonstrated the highest antioxidant activity, possibly attributed to the increased amount of bound ACN in BCP. While our primary focus is on using blackcurrant ACN as a pH indicator for monitoring food quality, its antioxidant capabilities could also be harnessed to extend the shelf life of food products.

https://doi.org/10.1021/acssuschemeng.5c05240
ACS Sustainable Chem. Eng. 2025, 13, 13988−14002

Table 6. CIE Lab Color Analysis of NaAlg and NaAlg−BCP Films after Exposure to 10% v/v CH_3COOH and NH_3 for 6 h[a]

conditions	sample	color attributes			color difference (ΔE)
		L^*	a^*	b^*	
control at t_0	NaAlg	64.67 ± 0.58^{Aa}	-0.33 ± 0.58^{Ac}	4.33 ± 0.58^{Ac}	n/a
	NaAlg−BCP10	54.67 ± 0.58^{Ad}	0.33 ± 0.58^{Abc}	11.00 ± 0.01^{Bb}	n/a
	NaAlg−BCP20	57.67 ± 0.58^{Abc}	1.33 ± 0.58^{Cb}	9.67 ± 0.58^{Cbc}	n/a
	NaAlg−BCP50	51.67 ± 0.58^{Ae}	3.67 ± 0.58^{Ba}	14.67 ± 0.58^{Ca}	n/a
	NaAlg−DFC	58.67 ± 0.58^{Ab}	0.00 ± 0.01^{Cbc}	8.33 ± 0.58^{Cc}	n/a
	NaAlg−ACN	56.00 ± 0.01^{Acd}	1.00 ± 0.01^{Bbc}	10.33 ± 0.58^{Bb}	n/a
10% CH_3COOH, 6 h	NaAlg	64.67 ± 0.58^{Aa}	0.00 ± 0.01^{Ac}	4.67 ± 0.58^{Ae}	0.94 ± 0.82^{Ab}
	NaAlg−BCP10	54.33 ± 0.58^{Ac}	1.00 ± 0.01^{Abc}	11.67 ± 0.58^{Bbc}	1.05 ± 0.92^{Bb}
	NaAlg−BCP20	55.67 ± 0.58^{Abc}	3.67 ± 0.58^{Ba}	13.33 ± 0.58^{Bb}	4.87 ± 0.66^{Bab}
	NaAlg−BCP50	52.33 ± 0.58^{Ad}	4.67 ± 0.58^{Ba}	16.67 ± 0.58^{Ba}	2.49 ± 1.10^{Bab}
	NaAlg−DFC	57.00 ± 0.01^{Ab}	2.00 ± 0.01^{Bb}	11.00 ± 0.01^{Bcd}	3.75 ± 0.65^{Bab}
	NaAlg−ACN	57.00 ± 0.01^{Ab}	1.00 ± 0.01^{Bbc}	9.67 ± 0.58^{Bd}	1.28 ± 1.43^{Bb}
10% NH_3, 6 h	NaAlg	66.33 ± 0.58^{Aa}	0.00 ± 0.01^{Ad}	4.00 ± 0.01^{Ad}	1.91 ± 1.01^{Ad}
	NaAlg−BCP10	56.00 ± 0.01^{Ab}	1.33 ± 0.58^{Ad}	21.00 ± 0.01^{Ac}	10.15 ± 0.09^{Ac}*
	NaAlg−BCP20	43.67 ± 0.58^{Bc}	7.67 ± 0.58^{Ab}	36.00 ± 0.01^{Aa}	30.50 ± 0.84^{Aa}*
	NaAlg−BCP50	29.67 ± 1.15^{Bd}	13.33 ± 0.58^{Aa}	34.67 ± 0.58^{Aa}	31.28 ± 1.52^{Aa}*
	NaAlg−DFC	45.00 ± 0.01^{Bc}	5.00 ± 0.01^{Ac}	31.33 ± 0.58^{Ab}	27.22 ± 1.11^{Ab}*
	NaAlg−ACN	45.00 ± 1.00^{Bc}	5.00 ± 0.01^{Ac}	32.33 ± 0.58^{Ab}	24.93 ± 1.17^{Ab}*

[a]Values are presented as mean ± SD ($n = 3$). Different lowercase letters (a−e) indicate significant differences ($p < 0.05$) between films under the same conditions. Different uppercase letters (A−C) indicate the significant differences ($p < 0.05$) for the same film under different conditions. $\Delta E > 5$ (*) indicates a color difference noticeable to the human eye.

Table 7. CIE Lab Color Analysis of the NaAlg−BCP50 Film after Exposure to NH_3 at Varying Concentrations, Ranging from 10% v/v to 500 ppm, for 2 and 6 h[a]

conditions	sample	color attributes			color difference (ΔE)
		L^*	a^*	b^*	
10% NH_3, 6 h	NaAlg−BCP50	29.67 ± 1.15^{Ac}	13.33 ± 0.58^{Aa}	34.67 ± 0.58^{Aa}	31.28 ± 1.52^{Aa}*
5% NH_3, 6 h	NaAlg−BCP50	36.67 ± 0.58^{Bb}	5.00 ± 0.01^{Ab}	29.00 ± 0.01^{Ab}	20.80 ± 0.44^{Ab}*
1% NH_3, 6 h	NaAlg−BCP50	46.67 ± 0.58^{Ba}	0.33 ± 0.58^{Ac}	21.33 ± 0.58^{Ac}	9.01 ± 0.79^{Ac}*
500 ppm of NH_3, 6 h	NaAlg−BCP50	45.67 ± 0.58^{Ba}	3.67 ± 0.58^{Ab}	19.33 ± 0.58^{Ad}	7.61 ± 0.35^{Ac}*
10% NH_3, 2 h	NaAlg−BCP50	29.67 ± 0.58^{Ac}	8.33 ± 0.58^{Ba}	35.67 ± 0.58^{Aa}	30.78 ± 0.79^{Aa}*
5% NH_3, 2 h	NaAlg−BCP50	40.00 ± 0.01^{Ab}	1.00 ± 0.01^{Bc}	27.00 ± 0.01^{Bb}	17.20 ± 0.63^{Bb}*
1% NH_3, 2 h	NaAlg−BCP50	49.00 ± 0.01^{Aa}	-0.67 ± 0.58^{Ad}	18.67 ± 0.58^{Bc}	6.54 ± 0.64^{Bc}*
500 ppm of NH_3, 2 h	NaAlg−BCP50	50.67 ± 0.58^{Aa}	4.67 ± 0.58^{Ab}	19.33 ± 0.58^{Ac}	4.96 ± 0.33^{Bc}

[a]Values are presented as mean ± SD ($n = 3$). Different lowercase letters (a−e) indicate significant differences ($p < 0.05$) between films exposed to different NH_3 concentrations at the same exposure time. Different uppercase letters (A−C) indicate the significant differences ($p < 0.05$) for the same film exposed to similar NH_3 concentrations at different exposure times. $\Delta E > 5^{(*)}$ indicates the observer may notice the difference between two colors.

Table 8. CIE Lab Color Analysis of the NaAlg−BCP50 Film Following Sequential Exposure to 10% NH_3 and 10% CH_3COOH, for 2 and 6 h[a]

conditions	sample	color attributes			color difference (ΔE)
		L^*	a^*	b^*	
at t_0	NaAlg−BCP50 after 6 h of 10%NH_3 exposure	28.67 ± 1.15^{c}	13.33 ± 0.58^{b}	34.67 ± 0.58^{b}	n/a
10%CH_3COOH, 2 h		42.67 ± 0.58^{b}	15.67 ± 0.58^{a}	40.00 ± 1.00^{a}	15.54 ± 0.90^{a}*
10%CH_3COOH, 6 h		46.00 ± 0.01^{a}	15.67 ± 0.58^{a}	41.67 ± 0.58^{a}	18.88 ± 1.11^{a}*

[a]Values are presented as mean ± SD ($n = 3$). Different lowercase letters (a−c) indicate significant differences ($p < 0.05$) between films exposed to the same CH_3COOH concentration at different exposure times. $\Delta E > 5$ (*) indicates a color difference perceptible to the human eye.

2.9. Volatile NH_3 and CH_3COOH Detection. Aqueous CH_3COOH and NH_3 solutions were prepared at a concentration of 10%v/v to demonstrate the ability of NaAlg and NaAlg−BCP films to detect volatile acids and amines within packaging environments. Figure S6 shows the color changes of the NaAlg−BCP films after 6 h of exposure to CH_3COOH and NH_3. A color change in response to NH_3 is seen in all NaAlg−BCP films, although the ACN fraction had not blended in films such as NaAlg−BCP10, NaAlg−BCP20, and NaAlg−BCP50. The observed color change can be attributed to the conversion of ACN[35] molecules into chalcone molecules due to an increase in pH from the addition of NH_3.[21,34,35] In addition, the darkening of the brown color may be a result of the ionization of the phenolic hydroxyl groups in an alkaline system, which has also been observed in the polyhydroxyalkanoate/tannin films.[42] In contrast, CH_3COOH

https://doi.org/10.1021/acssuschemeng.5c05240
ACS Sustainable Chem. Eng. 2025, 13, 13988−14002

Table 9. CIE Lab Color Analysis of NaAlg−BCP50 over a 14-Day Period[a]

sample	conditions	color attributes			color difference (ΔE)
		L^*	a^*	b^*	
NaAlg−BCP50	day 0	61.67 ± 1.53^{a}	13.00 ± 0.01^{b}	12.67 ± 0.58^{ab}	n/a
	day 1	63.33 ± 1.53^{ab}	12.00 ± 0.01^{ab}	12.00 ± 0.01^{a}	2.10 ± 0.60^{a}
	day 2	63.33 ± 0.58^{ab}	12.33 ± 0.58^{ab}	13.33 ± 0.58^{abc}	2.29 ± 1.63^{a}
	day 3	63.67 ± 0.58^{ab}	11.33 ± 0.58^{ab}	13.33 ± 0.58^{abc}	2.85 ± 0.56^{a}
	day 4	63.00 ± 1.00^{ab}	12.00 ± 1.00^{ab}	14.33 ± 0.58^{bcde}	2.74 ± 0.87^{a}
	day 5	63.00 ± 0.01^{ab}	12.33 ± 0.58^{ab}	14.67 ± 0.58^{bcde}	2.91 ± 0.58^{a}
	day 6	63.33 ± 0.58^{ab}	10.33 ± 0.58^{a}	14.00 ± 0.01^{abcd}	3.68 ± 0.48^{ab}
	day 7	64.00 ± 0.01^{b}	10.67 ± 0.58^{a}	15.33 ± 0.58^{cdef}	4.36 ± 1.23^{ab}
	day 8	64.00 ± 0.01^{b}	11.67 ± 1.15^{ab}	16.00 ± 1.00^{defg}	4.51 ± 1.01^{abc}
	day 9	64.00 ± 1.00^{b}	12.00 ± 1.00^{ab}	16.33 ± 0.58^{efg}	4.57 ± 0.44^{abc}
	day 10	64.33 ± 0.58^{b}	11.33 ± 0.58^{ab}	17.33 ± 0.58^{fghi}	5.71 ± 0.79^{bcd}*
	day 11	64.00 ± 0.01^{b}	10.33 ± 0.58^{a}	17.00 ± 1.00^{fgh}	5.74 ± 1.23^{bcd}*
	day 12	64.00 ± 0.01^{b}	11.33 ± 0.58^{ab}	17.67 ± 0.58^{ghi}	5.90 ± 0.52^{bcd}*
	day 13	64.33 ± 0.58^{b}	10.67 ± 1.53^{a}	18.67 ± 1.15^{hi}	7.16 ± 0.84^{cd}*
	day 14	64.33 ± 0.58^{b}	10.67 ± 0.58^{a}	19.33 ± 0.58^{i}	7.72 ± 1.04^{d}*

[a]Values are presented as mean ± SD (n = 3). Different lowercase letters (a−i) indicate significant differences ($p < 0.05$) between films over 14 days. $\Delta E > 5$ (*) indicates a color difference perceptible to the human eye.

vapor did not cause significant changes in the film color. This may be due to the pH of CH_3COOH being 3−4, which cannot drive the ACN molecules into the red flavylium cation structure occurring at pH below 3.[21,34,35] Additionally, the International Commission on Illumination (CIE) Lab color analysis confirmed a significant change in the color of NaAlg−BCP films (Tables 6, 7, and 8). The ΔE was >5, indicating that the change could be differentiated by the naked eye for all of the NaAlg−BCP films under NH_3 detection (Figure S6), and the NaAlg−BCP50 film displayed the most significant change (Table 6).

Further tests with various concentrations of NH_3 solutions (Table 7) were performed on the NaAlg−BCP50 film. The color change became visible after 2 h of exposure to NH_3 solution, with the light red-brown color intensifying into a dark brown upon prolonged exposure to NH_3 vapors. A concentration of 500 ppm of NH_3 was selected to demonstrate the spoilage environment of minced beef or pork, corresponding to the upper limit of the biogenic amine index, which is 500 mg/kg or 500 ppm.[60] This concentration was the lowest level found to induce a visible color change in the NaAlg−BCP50 film within 6 h, with a ΔE value of 7.61. Therefore, the NaAlg−BCP50 film has the potential to detect pork or beef spoilage within 6 h.

To demonstrate the reusability of NaAlg−BCP films for pH detection, a color-reversible test was performed on the NaAlg−BCP50 film. The film was sequentially exposed to 10% NH_3 for 6 h, followed by 10% CH_3COOH. Within 2 h of exposure to CH_3COOH, a visible color change was observed, shifting from dark brown to pale brown (Table 8 and Figure S6). However, the film cannot fully revert to its original color. This incomplete recovery can be explained by the sensitivity of ACN, which can be degraded under high-pH conditions.[35]

2.10. Stability of ACN within the Films. The stability of ACN can be influenced by various factors such as pH, temperature, light, antioxidants, oxygen, and the like.[61] Due to their excellent pH sensitivity, ACN incorporated into NaAlg−BCP films show successfully demonstrated visible color changes when exposed to NH_3, representing a high-pH environment. However, several other factors may affect the stability of ACN within the film matrix. Therefore, the NaAlg−BCP50 film was selected for further stability testing to evaluate how the film's color changes over a 14-day period and can be seen in Figure S7. CIE Lab color analysis (Table 9) confirmed a gradual color change in the NaAlg−BCP50 film, with the ΔE value increasing steadily with each day. A noticeable visual difference in color was observed within 10 days ($\Delta E > 5$). As the film was stored in an incubator at 25 °C, its color change may have been influenced by temperature, light, and air exposure. ACNs are known to be more stable at lower temperatures (2−4 °C).[61,62] The observed brownish coloration can be attributed to the ring opening of ACN into chalcones at elevated temperatures.[63] Moisture in the air can also promote the deglycosylation of ACN into anthocyanidin glycosides, which can then convert into chalcones.[63] Oxygen is another critical factor affecting ACN stability, as its presence can lead to degradation through oxidative reactions or enzymatic activity involving oxidases.[64] Light, particularly high-intensity or UV light, can also induce ring opening of ACN into chalcones.[61] However, in this study, light was likely not the primary factor contributing to the film's color change, as the samples were stored in an incubator exposed only to natural light. As a result, the ACN in the film is not stable under ambient conditions, with color changes occurring within 10 days. Thus, the films should be stored under low-temperature, low-light, and low-oxygen conditions to preserve their stability and color integrity.

2.11. Thermal Stability of Films. The DSC profiles of NaAlg−BCP films revealed a small endothermic peak and a predominant sharp endothermic peak (Figure S8-B). As the BCP content in the films increased, the small endothermic peaks shifted to higher temperatures (from 147 to 152 °C), while the main sharp peak shifted lower (from 204 to 187 °C). This shift is likely due to the interference caused by the branches of pectin or ACN-bound pectin in BCP, which hinders the formation of the "egg box" structure. Moreover, incorporating DFC or ACN into NaAlg−BCP20 films did not affect the small endothermic peak at 150 °C. However, the main endothermic peak shifted higher to 195 °C with DFC addition and lower to 189 °C when ACN was incorporated. These findings suggest that no significant thermal transitions occur below 187 °C, indicating that all NaAlg−BCP films are

https://doi.org/10.1021/acssuschemeng.5c05240
ACS Sustainable Chem. Eng. 2025, 13, 13988−14002

well-suited for room temperature storage and relatively high-temperature food heating applications.

2.12. Green Aspects. The integrated microwave hydrothermal extraction at 100 °C successfully yielded ACN, BCP, and DFC from blackcurrant pomace, with each component functionally involved in the final film products. The total recovery yield of the three components was approximately 38%, comprising 4.42% ACN, 2.36% BCP, and 31.35% DFC. However, the nonrecovery part accounted for 61.87%, primarily composed of alkaline-resolved lignin (from the bleaching process) and low-molecular-weight carbohydrates such as sugars derived from hydrothermal hydrolysis of carbohydrate matters (from microwave hydrothermal treatment). Sugars can serve as bioderived acids or biofuel feedstock,[65,66] while lignin can be considered as a source of antioxidants, hydrophobic biobased additives, or bioenergy source.[59,67,68] This multistream valorization of blackcurrant pomace highlights the potential of a zero-waste biorefinery approach.

In comparison to conventional extraction methods, microwave hydrothermal treatment significantly reduced processing time from 2 h to 15 min of holding time and eliminates the need for harsh acids or organic solvents. In this study, microwave hydrothermal extraction has shown a lower energy consumption of approximately four times compared with conventional extraction (Table S2), supporting its environmental benefits.

Moreover, the NaAlg and NaAlg−BCP films are composed of biodegradable polysaccharides and natural colorants, suggesting favorable degradation under natural or composting conditions. The degradation is expected to proceed primarily via microbial breakdown of alginate, pectin, and cellulose, leaving no toxic residues[69,70] and making these films a sustainable option for short-term applications such as smart packaging.

3. CONCLUSIONS

Blending ACN, BCP, and DFC derived from blackcurrant pomace within a NaAlg matrix can produce pH-sensitive biobased films for potential food applications. These colorimetric films can detect NH_3 as a proxy for food freshness monitoring. Their antifogging properties, supported by high WVP, make them especially suitable for packaging highly perishable produce. Rheological studies revealed that NaAlg−BCP50 exhibited the most solidlike behavior, highest recovery, and highest tensile strength among all NaAlg−BCP films, making it potentially useful for applications requiring structural integrity under stress. However, for a wider range of commercial applications, the tensile strength of the prepared films based on NaAlg needs to be improved and the oxygen permeability and barrier properties need to be explored.[49] By leveraging BCP-derived components, the study highlights a sustainable approach to reducing food waste, enhancing food safety, and committing to responsible production and consumption. Moreover, the feasibility of using blackcurrant pomace as a multifunctional raw material is demonstrated through the use of microwave-assisted hydrothermal treatment, which consumes approximately four times less energy than conventional extraction methods, offering a more environmentally friendly alternative.

4. EXPERIMENTAL SECTION

4.1. Materials and Methods. All chemicals utilized in this research were supplied by Fisher, Sigma-Aldrich (now known as Merck Ltd.), and VWR chemical companies without any further purification. Dried blackcurrant pomace, consisting of seed, skin, stalk, and stem, was ground and sieved through a stainless steel mesh with a diameter of ≤2 mm. BCP and DFC were obtained from our previous study through microwave-assisted hydrothermal treatment at 100 °C.[7] Statistical analysis was performed on a one-way analysis of variance (ANOVA) with Tukey's test at a 0.05 significance level using the IBM SPSS Statistics program (version 29.0.2.0).

4.2. ACN Extraction. *4.2.1. 1:1 Ethanol−Water Extraction (Control).* Milled blackcurrant pomace (40 g) and solvent (200 mL; 1:1 ethanol/water) were heated under reflux for 2 h. The filtrate was evaporated and freeze-dried to dryness. The ethanol−water extract was stored in a closed vial and labeled as ETW.

4.2.2. Microwave Hydrothermal Extraction (MW100−160). Milled blackcurrant pomace (20 g) and deionized water (300 mL) were placed into a PTFE microwave vessel and subjected to microwave irradiation (Milestone Synthwave Microwave, 2.45 GHz magnetron frequency, 1500 W) at various temperatures (100, 120, 140, or 160 °C) for a 15 min ramp time and 15 min hold time, under 10 bar nitrogen and at 60% stirring. Thereafter, the filtrates were centrifuged, and the supernatants were retained for pectin precipitation by adding ethanol (1:2 supernatant/ethanol) and then kept in the refrigerator at 4 °C overnight. The BCP pellet was isolated from the supernatant by centrifugation. The supernatants, containing the ACN pigment, were evaporated and freeze-dried for further characterization and labeled as MW100, MW120, MW140, or MW160.

4.3. Film Fabrication. NaAlg−BCP aqueous solutions (4 wt % in 30 mL of deionized water) of ratios of 100:0, 90:10, 80:20, and 50:50 were prepared and stirred vigorously (800 rpm) at 40 °C for 3 h. Thereafter, glycerol (0.625 g), DFC suspension (0% or 2 wt %, 1.25 mL), and ACN solution (0% or 0.5 wt %, 1.25 mL) were added to the polymer mixture. The entire mixture was then stirred at 800 rpm and 40 °C for 30 min. Thereafter, the mixture was sonicated in degas mode at room temperature for 20 min and carefully poured into 9 mm diameter Petri dishes (10 g) and set to cast in an oven at 50 °C for 20 h.

Filter papers (9 mm diameter) were soaked overnight in a 0.5% $CaCl_2$−7%glycerol solution, removed, and placed on top of the previously oven-dried films for 2 min to facilitate cross-linking. The cross-linked films were dried in a fume hood at ambient temperature overnight and then stored in plastic zip-lock bags. The prepared films were labeled as shown in Table 10.

Table 10. Composition of NaAlg−BCP Films

sample code	NaAlg/BCP ratio	additives (%)
NaAlg	100:0	-
NaAlg−BCP10	90:10	-
NaAlg−BCP20	80:20	-
NaAlg−BCP50	50:50	-
NaAlg−DFC	80:20	DFC (2%)
NaAlg−ACN	80:20	ACN (0.5%)

4.4. Characterization of Blackcurrant Pomace Hydrolysate. *4.4.1. Determination of Total Phenolic Content.* The total phenolic content in the blackcurrant hydrolysate was determined following a modified literature method.[71] Gallic acid solution/sample solution (0.5 mL) was mixed with 1 N Folin−Ciocalteu reagent (0.5 mL). Na_2CO_3 solution (2%w/v, 9 mL) was added to the mixture and allowed to stand for 25 min at room temperature. The final concentrations of gallic acid solution were 0, 0.002, 0.004, 0.006, 0.008, and 0.010 mg/mL. A standard curve was plotted ($y = 99.043x + 0.084$, $R^2 = 0.9998$), and the contents of phenolic compounds were measured at 730 nm using UV−vis spectroscopy with deionized water

https://doi.org/10.1021/acssuschemeng.5c05240
ACS Sustainable Chem. Eng. 2025, 13, 13988−14002

as the reference. The result was expressed as milligrams of gallic acid (GA) equivalents per gram of dried weight sample (mg GA/g dry weight). The total phenolic content (TPC) of the extracts was calculated using the following equation

$$\mathrm{TPC} = \frac{c \times V}{m}$$

where c is the sample concentration before dilution (mg/mL), V is the volume (mL) of the solvent used for dissolving, and m is the weight (g) of the dried sample.

4.4.2. Determination of Total Anthocyanin Content. The total anthocyanin content was determined according to the AOAC protocol.[72,73] Blackcurrant hydrolysate samples were prepared at a concentration of 1 mg/mL. One portion (1.5 mL) of the hydrolysate was mixed with potassium chloride buffer (0.2 M, pH 1.0, 1 mL), and another portion (1.5 mL) was mixed with sodium acetate buffer (0.2 M, pH 4.5, 1 mL). Then, the mixtures were diluted by adding deionized water (2 mL), and absorbance was recorded using a Jasco 500 UV−visible spectrophotometer at wavelengths of 520 and 700 nm, for solutions at pH 1.0 and 4.5, respectively. The total anthocyanin content (TAC) was expressed as cyanidin-3-glucoside equivalents (C3G mg/g) and was calculated using the following equation

$$\mathrm{TAC}\left(\mathrm{C3G}\frac{\mathrm{mg}}{\mathrm{g}}\right) = \frac{A \times MW \times DF \times V}{\varepsilon \times l \times W}$$

where A is $(A_{520\ \mathrm{nm}} - A_{700\ \mathrm{nm}})_{\mathrm{pH1.0}} - (A_{520\ \mathrm{nm}} - A_{700\ \mathrm{nm}})_{\mathrm{pH4.5}}$, MW is the molecular weight of C3G (449.2 g/mol), DF is the dilution factor, V is the volume of the solvent (mL), W is the sample weight (mg), l is the path length (cm), and ε is the molar extinction coefficient of C3G (26,900 L/mol·cm).

4.4.3. Antioxidant Activity Based on the DPPH Assay. The DPPH assay was carried out using the method reported by Do et al.[74] Blackcurrant hydrolysates (0.12 mg/mL, 2.5 mL) were mixed with DPPH solution (0.3 mM, 2.5 mL). The mixtures were incubated for 20 min in a dark area at room temperature. The absorbance of mixtures was measured at 517 nm using a Jasso 500 UV−visible spectrophotometer. Ethanol was used as a reference. DPPH inhibition was calculated by the following equation

$$\text{DPPH inhibition (\%)} = \frac{A_{\mathrm{control}} - A_{\mathrm{sample}}}{A_{\mathrm{control}}} \times 100$$

where A_{control} is the absorbance of the mixture of ethanol and DPPH solution and A_{sample} is the absorbance of the mixture of the sample extract and DPPH solution.

4.4.4. UV−Visible (UV−Vis) Spectroscopy Analysis. The pH-responsive color of the blackcurrant hydrolysates was investigated by measuring their absorption spectra in buffer solutions from pH 1 to 11. The spectra were determined by using a Jasso 500 UV−visible spectrophotometer from 400 to 700 nm.

4.5. Characterization of Films. *4.5.1. Microstructure Analysis.* The microstructure study of films was conducted using a scanning electron microscope (JEOL JSM 7800F Prime field-emission gun scanning electron microscope, FEGSEM) at a 5 kV accelerating voltage and a magnification of 1000 and 4000×.

Samples were prepared by mounting on 12.5 mm diameter aluminum pin stubs (Agar Scientific U.K. Ltd.) using carbon-rich self-adhesive discs (Agar Scientific U.K. Ltd.). Cross sections were prepared by cryofracturing with liquid nitrogen. All of the mounted samples were sputter-coated with platinum in a Safematic CCU-10 sputter coater.

4.5.2. ATR-IR Analysis. ATR-IR analysis of film samples was performed using a PerkinElmer Spectrum 400 IR. The spectra were scanned and recorded from 4000 to 600 cm^{-1}, with the force gauge between 100 and 120 and four scans per sample.

4.5.3. Mechanical Properties. The tensile properties were evaluated using an Instron 3367 device (Instron). Dog bone-shaped specimens (20 mm in length and 3 mm in width) were obtained from the films and tested at a speed of 4 mm/min. The tensile properties were determined based on the thickness of the film, which was calculated for each sample using the mean thickness. The results are presented as mean values and standard deviations derived from five measurements.

4.5.4. Rheological Study. Flow curves, amplitude sweep and frequency sweep analysis, and creep and recovery tests were conducted with a Kinexus rheometer (Malvern Instruments Ltd., Malvern, U.K.) equipped with a cone plate measuring system (CP4/40, 40 mm diameter, 0.1448 mm gap) at 25 °C. Flow curves were measured from 1 to 1000 s^{-1} in 2 min. The amplitude sweep test was conducted at an angular frequency (ω) of 1 Hz and shear strain (γ) ranging from 0.1 to 100%. The frequency sweep test was evaluated at a shear strain of 0.5% (within the LVR) and a frequency ranging from 0.1 to 10 Hz. Creep and recovery tests were conducted at a gap of 1 mm by the step test while applying a shear stress of 0.5 Pa for 180 s, followed by removing the shear stress for 180 s to observe the strain recovery.

4.5.5. Physical Properties. Film thickness was measured with a digital micrometer at 17 different points within every 1 cm interval across the film samples. The moisture content was calculated using the following equation and measured four times for each sample

$$\text{moisture content (\%)} = \frac{W_0 - W}{W_0} \times 100$$

where W_0 is the initial weight of the film and W is the weight of film after drying.

4.5.6. Water Contact Angle Analysis. The hydrophilicity of the film was measured by an Attension Theta tensiometer using the sessile drop analysis and Young−Laplace analysis mode. Films were cut into (1 cm × 1 cm) pieces, and deionized water droplets (1 μL) were dropped on each film sample. Each sample was measured five times in an ambient atmosphere. Water contact angle analysis was performed using the ImageJ program (version 1.54g) with a drop analysis plugin.

4.5.7. Water Vapor Transmission Properties. The WVTR and WVP of the NaAlg−BCP films were measured using the dry cup method, modified according to Azmi et al.[52] and based on the ASTM E96 standard. Glass vials with a transmission area of 64 mm^2 were used for the measurement. The NaAlg−BCP films were placed in a desiccator maintained at 25 °C with a saturated magnesium nitrate solution to control the relative humidity at 50 ± 5% for 24 h. A digital ThermoPro TP49 hygrometer (ThermoPro, China) was placed inside the desiccator to monitor the real-time temperature and humidity. Anhydrous calcium chloride was added to the vial to maintain a relative humidity of 0%. Silicone grease was applied to the rim of the vial, and the NaAlg−BCP films were placed on top. The initial weight of the vial with the films was recorded, after which the vial was stored in a desiccator maintained at 50% RH and 25 °C. The weight of the vial was monitored daily for 7 days. The WVTR and WVP were calculated using the following equation

$$\mathrm{WVTR} = \frac{\Delta m}{\Delta t \cdot A}$$

$$\mathrm{WVP} = \mathrm{WVTR}\left(\frac{L}{\Delta p}\right)$$

where $\frac{\Delta m}{\Delta t}$ is the weight gain over time, A is the transmission area of the film, L is the film thickness, and Δp is the difference in water vapor partial pressure across the film.[75]

4.5.8. Fogging Test. The antifogging property of NaAlg−BCP films was investigated using the hot-fog test.[76] A volume of 0.75 ml of water was added to a 3 mL vial, and silicone grease was applied to the rim to ensure a proper seal. The NaAlg−BCP films were then placed in the vial openings. The vial was heated to 60 °C for 3 h to induce condensation. The transparency of each sample was visually evaluated and scored on a scale from A (completely transparent) to D (fully

https://doi.org/10.1021/acssuschemeng.5c05240
ACS Sustainable Chem. Eng. 2025, 13, 13988−14002

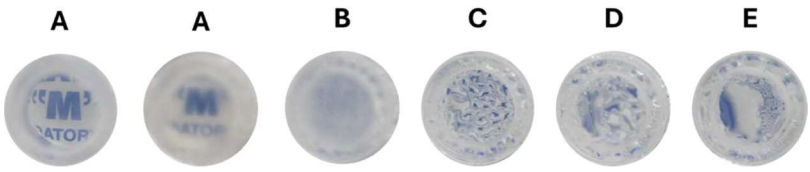

Figure 5. Pictures of different scores based on surface appearance after the fogging test: (A) transparent surface, (B) fogging surface with reduced transparency, (C) fogging surface exhibiting small, discrete water droplets, (D) surface with reduced transparency and medium-sized, discrete water droplets, and (E) surface exhibiting coalesced water droplets.

fogged with coalesced water droplets) (Figure 5). A glass slide was used as a control.

4.5.9. Antioxidant Activity. The antioxidant activity of the films was investigated by the DPPH assay.[42,74] The absorbance of a freshly prepared DPPH solution in ethanol (0.025 mM) was measured at 517 nm ($A_{control}$). Then, small pieces of the films (0.3 cm × 2.0 cm) were placed in the DPPH solution and incubated in a dark area for 1 h. The absorbance of each film (A_{sample}) in the DPPH solution was measured using a Jasco 500 spectrophotometer at 517 nm with a resolution of 0.5 nm after 1 h of incubation. DPPH inhibition was calculated using the following equation

$$\text{DPPH inhibition (\%)} = \frac{A_{control} - A_{sample}}{A_{control}} \times 100$$

4.5.10. CH_3COOH and NH_3 Detection. The capability of the films to detect CH_3COOH and NH_3 vapor was evaluated using the method described by Ferri et al.[42] The films were cut and put into the hole of the vial cap, containing CH_3COOH or NH_3 solution (10%v/v, 2 mL). The vials were allowed to stand in the fume hood for 6 h to investigate any color change of the films. The NaAlg−BCP50 film was selected for further sensitivity testing with varying concentrations (500 ppm, 1, 5, 10%v/v) of NH_3. The NaAlg−BCP50 film after exposure under NH_3 (10%v/v, 6 h) was chosen for the color-reversible test with CH_3COOH (10%v/v). The color transitions were quantified by using the CIE Lab color space system, which measures colors with Cartesian coordinates (L^*, a^*, and b^*). Photos were taken under consistent conditions, and the total color difference (ΔE) was calculated using the following equation

$$\Delta E = \sqrt{(L_{1^*} - L_{2^*})^2 + (a_{1^*} - a_{2^*})^2 + (b_{1^*} - b_{2^*})^2}$$

when the value of the ΔE is greater than 5, the observer can clearly perceive two different colors.

4.5.11. Stability of ACN within the Films. Freshly prepared NaAlg−BCP50 films (n = 3) were used to investigate color changes over time. Prior to analysis, photographs of the films were taken and recorded on day 0. The films were then stored in an incubator at 25 °C and photographed daily at 24 h intervals for 14 days. Color measurements were quantified by using the CIE Lab color space system. All photographs were taken under consistent lighting and camera settings to ensure accuracy.

4.5.12. Thermal Stability. Differential scanning calorimetry was conducted using MDSC, TA Instruments. The film samples (about 5−6 mg) were heated in a hermetically sealed aluminum pan under a nitrogen atmosphere, from 40 to 300 °C at a heating rate of 10 °C/min. An empty sealed aluminum pan was used as a reference, and the instrument was calibrated with an indium standard.[17]

■ ASSOCIATED CONTENT

Supporting Information

The Supporting Information is available free of charge at https://pubs.acs.org/doi/10.1021/acssuschemeng.5c05240.

Process diagram of blackcurrant pomace fractionation and film fabrication, LC−MS analysis of anthocyanins, flow curves of film-forming solutions, water contact angle images of films, DSC thermograms, and images illustrating film's color changes (PDF)

■ AUTHOR INFORMATION

Corresponding Author

Avtar Singh Matharu − *Green Chemistry Centre of Excellence, Department of Chemistry, University of York, York YO10 5DD, United Kingdom;* orcid.org/0000-0002-9488-565X; Email: Avtar.Matharu@york.ac.uk

Authors

Natthamon Inthalaeng − *Green Chemistry Centre of Excellence, Department of Chemistry, University of York, York YO10 5DD, United Kingdom;* orcid.org/0000-0002-5494-095X

Thomas Iain James Dugmore − *Green Chemistry Centre of Excellence, Department of Chemistry, University of York, York YO10 5DD, United Kingdom;* orcid.org/0000-0003-3741-0276

Complete contact information is available at: https://pubs.acs.org/10.1021/acssuschemeng.5c05240

Author Contributions

N.I.: designed, planned, and investigated the research and original draft writing. T.D.: secondary supervision. A.M.: primary supervision, scientific discussion, and manuscript reviewing and editing. All authors have given approval to the final version of the manuscript.

Notes

The authors declare no competing financial interest.

■ ACKNOWLEDGMENTS

The financial support by the Development and Promotion of Science and Technology Talents Project (DPST) under the Royal Thai Government (Grant No. DPST582042) is acknowledged. The authors also thank Paul Gunning (Biosciences Technology Facility, University of York) for providing the SEM images of films.

■ ABBREVIATIONS

ACN, anthocyanin; ANOVA, one-way analysis of variance; ATR-IR, attenuated total reflectance Fourier transform infrared; BAI, biogenic amine index; BCP, blackcurrant pectin; CH_3COOH, acetic acid; C3G, cyanidin-3-glucoside; C3R, cyanidin-3-rutinoside; D3G, delphinidin-3-glucoside; D3R, delphinidin-3-rutinoside; DFC, defibrillated cellulose; DPPH, 2,2-diphenyl-1-picrylhydrazyl; DSC, differential scanning calorimetry; ETW, ethanol−water extract; FCR, Folin−Ciocalteu reagent; GA, gallic acid; LVR, linear viscoelastic region; MW100, microwave at 100 °C extract; MW120, microwave at 120 °C extract; MW140, microwave at 140 °C extract; MW160, microwave at 160 °C extract; NaAlg, sodium alginate; NH_3, ammonia; SEM, scanning electron microscopy; TAC, total anthocyanin content; TPC, total phenolic content; WVP,

https://doi.org/10.1021/acssuschemeng.5c05240
ACS Sustainable Chem. Eng. 2025, 13, 13988−14002

water vapor permeability; WVTR, water vapor transmission rate

REFERENCES

(1) United Nations. Population. https://www.un.org/en/global-issues/population. (accessed May 14, 2025).

(2) United Nations Environment Programme. Food Waste Index Report . Think Eat Save: Tracking Progress to Halve Global Food Waste 2024 https://wedocs.unep.org/20.500.11822/45230. (accessed June 27, 2025).

(3) Teigiserova, D. A.; Hamelin, L.; Thomsen, M. Review of High-Value Food Waste and Food Residues Biorefineries with Focus on Unavoidable Wastes from Processing. *Resour., Conserv. Recycl.* **2019**, *149*, 413−426.

(4) Sulaeman, A. P.; Gao, Y.; Dugmore, T.; Remón, J.; Matharu, A. S. From Unavoidable Food Waste to Advanced Biomaterials: Microfibrilated Lignocellulose Production by Microwave-Assisted Hydrothermal Treatment of Cassava Peel and Almond Hull. *Cellulose* **2021**, *28* (12), 7687−7705.

(5) Alba, K.; MacNaughtan, W.; Laws, A. P.; Foster, T. J.; Campbell, G. M.; Kontogiorgos, V. Fractionation and Characterisation of Dietary Fibre from Blackcurrant Pomace. *Food Hydrocolloids* **2018**, *81*, 398−408.

(6) Cao, L.; Park, Y.; Lee, S.; Kim, D. O. Extraction, Identification, and Health Benefits of Anthocyanins in Blackcurrants (Ribes Nigrum l.). *Appl. Sci.* **2021**, *11* (4), No. 1863.

(7) Wądrzyk, M.; Plata, M.; Korzeniowski, L.; Janus, R.; Lewandowski, M. Towards sustainable valorization of blackcurrant pomace: Investigation of hot-water extraction combined with hydrothermal liquefaction. *Renewable Energy* **2025**, *240*, No. 122117.

(8) Inthalaeng, N.; Barker, R. E.; Dugmore, T. I. J.; Matharu, A. S. Microwave-Assisted Production of Defibrillated Lignocelluloses from Blackcurrant Pomace via Citric Acid and Acid-Free Conditions. *Molecules* **2024**, *29* (23), No. 5665.

(9) You, P.; Wang, L.; Zhou, N.; Yang, Y.; Pang, J. A PH-Intelligent Response Fish Packaging Film: Konjac Glucomannan/Carboxymethyl Cellulose/Blackcurrant Anthocyanin Antibacterial Composite Film. *Int. J. Biol. Macromol.* **2022**, *204*, 386−396.

(10) Luchese, C. L.; Sperotto, N.; Spada, J. C.; Tessaro, I. C. Effect of Blueberry Agro-Industrial Waste Addition to Corn Starch-Based Films for the Production of a PH-Indicator Film. *Int. J. Biol. Macromol.* **2017**, *104*, 11−18.

(11) Khalil, H. P. S. A.; Tye, Y. Y.; Chow, S. T.; Saurabh, C. K.; Tahir, P. M.; Dungani, R.; Syakir, M. I. Cellulosic Pulp Fiber as Reinforcement Materials in Seaweed-Based Film. *BioResources* **2017**, *12* (1), 29−42.

(12) Gao, Y.; Remón, J.; Matharu, A. S. Microwave-Assisted Hydrothermal Treatments for Biomass Valorisation: A Critical Review. *Green Chem.* **2021**, *23* (10), 3502−3525.

(13) Inthalaeng, N.; Dugmore, T. I. J.; Matharu, A. S. Production of Hydrogels from Microwave-Assisted Hydrothermal Fractionation of Blackcurrant Pomace. *Gels* **2023**, *9* (9), No. 674.

(14) Gao, Y.; Xia, H.; Sulaeman, A. P.; de Melo, E. M.; Dugmore, T. I. J.; Matharu, A. S. Defibrillated Celluloses via Dual Twin-Screw Extrusion and Microwave Hydrothermal Treatment of Spent Pea Biomass. *ACS Sustainable Chem. Eng.* **2019**, *7* (13), 11861−11871.

(15) Pap, N.; Beszédes, S.; Pongrácz, E.; Myllykoski, L.; Gábor, M.; Gyimes, E.; Hodúr, C.; Keiski, R. L. Microwave-Assisted Extraction of Anthocyanins from Black Currant Marc. *Food Bioprocess Technol.* **2013**, *6* (10), 2666−2674.

(16) Alchera, F.; Ginepro, M.; Giacalone, G. Microwave-Assisted Extraction of Polyphenols from Blackcurrant By-Products and Possible Uses of the Extracts in Active Packaging. *Foods* **2022**, *11* (18), No. 2727.

(17) Wang, Q.; Jiang, Y.; Chen, W.; McClements, D. J.; Ma, C.; Liu, X.; Liu, F. Development of PH-Responsive Active Film Materials Based on Purple Corncob and Its Application in Meat Freshness Monitoring. *Food Res. Int.* **2022**, *161*, No. 111832.

(18) Zhang, X.; Liu, Y.; Yong, H.; Qin, Y.; Liu, J.; Liu, J. Development of Multifunctional Food Packaging Films Based on Chitosan, TiO2 Nanoparticles and Anthocyanin-Rich Black Plum Peel Extract. *Food Hydrocolloids* **2019**, *94*, 80−92.

(19) Lei, Y.; Yao, Q.; Jin, Z.; Wang, Y.-C. Intelligent Films Based on Pectin, Sodium Alginate, Cellulose Nanocrystals, and Anthocyanins for Monitoring Food Freshness. *Food Chem.* **2023**, *404*, No. 134528.

(20) Liu, Y.; Qin, Y.; Bai, R.; Zhang, X.; Yuan, L.; Liu, J. Preparation of PH-Sensitive and Antioxidant Packaging Films Based on κ-Carrageenan and Mulberry Polyphenolic Extract. *Int. J. Biol. Macromol.* **2019**, *134*, 993−1001.

(21) Zhang, T.; Wang, H.; Qi, D.; Xia, L.; Li, L.; Li, X.; Jiang, S. Multifunctional Colorimetric Cellulose Acetate Membrane Incorporated with Perilla Frutescens (L.) Britt. Anthocyanins and Chamomile Essential Oil. *Carbohydr. Polym.* **2022**, *278*, No. 118914.

(22) Nešić, A.; Onjia, A.; Davidović, S.; Dimitrijević, S.; Errico, M. E.; Santagata, G.; Malinconico, M. Design of Pectin-Sodium Alginate Based Films for Potential Healthcare Application: Study of Chemico-Physical Interactions between the Components of Films and Assessment of Their Antimicrobial Activity. *Carbohydr. Polym.* **2017**, *157*, 981−990.

(23) Janik, W.; Nowotarski, M.; Ledniowska, K.; Shyntum, D. Y.; Krukiewicz, K.; Turczyn, R.; Sabura, E.; Furgoł, S.; Kudła, S.; Dudek, G. Modulation of Physicochemical Properties and Antimicrobial Activity of Sodium Alginate Films through the Use of Chestnut Extract and Plasticizers. *Sci. Rep.* **2023**, *13* (1), No. 11530.

(24) Dai, H.; Ou, S.; Huang, Y.; Huang, H. Utilization of Pineapple Peel for Production of Nanocellulose and Film Application. *Cellulose* **2018**, *25* (3), 1743−1756.

(25) Gohil, R. M. Synergistic Blends of Natural Polymers, Pectin and Sodium Alginate. *J. Appl. Polym. Sci.* **2011**, *120* (4), 2324−2336.

(26) Rezvanian, M.; Ahmad, N.; Amin, M. C. I. M.; Ng, S.-F. Optimization, Characterization, and in Vitro Assessment of Alginate-Pectin Ionic Cross-Linked Hydrogel Film for Wound Dressing Applications. *Int. J. Biol. Macromol.* **2017**, *97*, 131−140.

(27) Šimerdová, B.; Bobríková, M.; Lhotská, I.; Kaplan, J.; Křenová, A.; Šatínský, D. Evaluation of Anthocyanin Profiles in Various Blackcurrant Cultivars over a Three-Year Period Using a Fast HPLC-DAD Method. *Foods* **2021**, *10* (8), No. 1745.

(28) Nour, V.; Stampar, F.; Veberic, R.; Jakopic, J. Anthocyanins Profile, Total Phenolics and Antioxidant Activity of Black Currant Ethanolic Extracts as Influenced by Genotype and Ethanol Concentration. *Food Chem.* **2013**, *141* (2), 961−966.

(29) Laczkó-Zöld, E.; Komlósi, A.; Ülkei, T.; Fogarasi, E.; Croitoru, M.; Fülöp, I.; Domokos, E.; Ştefănescu, R.; Varga, E. Extractability of Polyphenols from Black Currant, Red Currant and Gooseberry and Their Antioxidant Activity. *Acta Biol. Hung.* **2018**, *69* (2), 156−169.

(30) Sadilova, E.; Carle, R.; Stintzing, F. C. Thermal Degradation of Anthocyanins and Its Impact on Color and in Vitro Antioxidant Capacity. *Mol. Nutr. Food Res.* **2007**, *51* (12), 1461−1471.

(31) Oancea, S. A Review of the Current Knowledge of Thermal Stability of Anthocyanins and Approaches to Their Stabilization to Heat. *Antioxidants* **2021**, *10*, No. 1337.

(32) Zhao, M.; Bai, J.; Bu, X.; Tang, Y.; Han, W.; Li, D.; Wang, L.; Yang, Y.; Xu, Y. Microwave-Assisted Aqueous Two-Phase Extraction of Phenolic Compounds from Ribes Nigrum L. and Its Antibacterial Effect on Foodborne Pathogens. *Food Control* **2021**, *119*, No. 107449.

(33) Milić, A.; Daničić, T.; Horecki, A. T.; Šumić, Z.; Teslić, N.; Kovačević, D. B.; Putnik, P.; Pavlić, B. Sustainable Extractions for Maximizing Content of Antioxidant Phytochemicals from Black and Red Currants. *Foods* **2022**, *11*, No. 325.

(34) Rose, P. M.; Cantrill, V.; Benohoud, M.; Tidder, A.; Rayner, C. M.; Blackburn, R. S. Application of Anthocyanins from Blackcurrant (Ribes Nigrum L.) Fruit Waste as Renewable Hair Dyes. *J. Agric. Food Chem.* **2018**, *66* (26), 6790−6798.

(35) Priyadarshi, R.; Ezati, P.; Rhim, J.-W. Recent Advances in Intelligent Food Packaging Applications Using Natural Food Colorants. *ACS Food Sci. Technol.* **2021**, *1* (2), 124−138.

https://doi.org/10.1021/acssuschemeng.5c05240
ACS Sustainable Chem. Eng. 2025, 13, 13988−14002

(36) Makaremi, M.; Yousefi, H.; Cavallaro, G.; Lazzara, G.; Goh, C. B.; Lee, S. M.; Solouk, A.; Pasbakhsh, P. Safely Dissolvable and Healable Active Packaging Films Based on Alginate and Pectin. *Polymers* **2019**, *11*, No. 1594.
(37) Kang, S.; Xiao, Y.; Guo, X.; Huang, A.; Xu, H. Development of Gum Arabic-Based Nanocomposite Films Reinforced with Cellulose Nanocrystals for Strawberry Preservation. *Food Chem.* **2021**, *350*, No. 129199.
(38) Wu, C.; Li, Y.; Sun, J.; Lu, Y.; Tong, C.; Wang, L.; Yan, Z.; Pang, J. Novel Konjac Glucomannan Films with Oxidized Chitin Nanocrystals Immobilized Red Cabbage Anthocyanins for Intelligent Food Packaging. *Food Hydrocolloids* **2020**, *98*, No. 105245.
(39) Cao, L.; Lu, W.; Mata, A.; Nishinari, K.; Fang, Y. Egg-Box Model-Based Gelation of Alginate and Pectin: A Review. *Carbohydr. Polym.* **2020**, *242*, No. 116389.
(40) Vityazev, F. V.; Khramova, D. S.; Saveliev, N. Y.; Ipatova, E. A.; Burkov, A. A.; Beloserov, V. S.; Belyi, V. A.; Kononov, L. O.; Martinson, E. A.; Litvinets, S. G.; Markov, P. A.; Popov, S. V. Pectin−Glycerol Gel Beads: Preparation, Characterization and Swelling Behaviour. *Carbohydr. Polym.* **2020**, *238*, No. 116166.
(41) Prietto, L.; Mirapalhete, T. C.; Pinto, V. Z.; Hoffmann, J. F.; Vanier, N. L.; Lim, L. T.; Dias, A. R. G.; da Rosa Zavareze, E. PH-Sensitive Films Containing Anthocyanins Extracted from Black Bean Seed Coat and Red Cabbage. *LWT* **2017**, *80*, 492−500.
(42) Ferri, M.; Papchenko, K.; Esposti, M. D.; Tondi, G.; De Angelis, M. G.; Morselli, D.; Fabbri, P. Fully Biobased Polyhydroxyalkanoate/Tannin Films as Multifunctional Materials for Smart Food Packaging Applications. *ACS Appl. Mater. Interfaces* **2023**, *15* (23), 28594−28605.
(43) Solberg, A.; Draget, K. I.; Schatz, C.; Christensen, B. E. Alginate Blocks and Block Polysaccharides: A Review. *Macromol. Symp.* **2023**, *408* (1), No. 2200072, DOI: 10.1002/masy.202200072.
(44) Singh, P.; Baisthakur, P.; Yemul, O. S. Synthesis, Characterization and Application of Crosslinked Alginate as Green Packaging Material. *Heliyon* **2020**, *6* (1), No. e03026, DOI: 10.1016/j.heliyon.2019.e03026.
(45) Sun, Y.; Liu, Z.; Zhang, L.; Wang, X.; Li, L. Effects of Plasticizer Type and Concentration on Rheological, Physico-Mechanical and Structural Properties of Chitosan/Zein Film. *Int. J. Biol. Macromol.* **2020**, *143*, 334−340.
(46) Basak, S.; Annapure, U. S. Rheological Performance of Film-Forming Solutions and Barrier Properties of Films Fabricated from Cold Plasma-Treated High Methoxyl Apple Pectin and Crosslinked by Ca2+: Impact of Plasma Treatment Voltage. *Int. J. Biol. Macromol.* **2023**, *227*, 938−951.
(47) Bélafi-Bakó, K.; Cserjési, P.; Beszédes, S.; Csanádi, Z.; Hodúr, C. Berry Pectins: Microwave-Assisted Extraction and Rheological Properties. *Food Bioprocess Technol.* **2012**, *5* (3), 1100−1105.
(48) Ma, J.; Lin, Y.; Chen, X.; Zhao, B.; Zhang, J. Flow Behavior, Thixotropy and Dynamical Viscoelasticity of Sodium Alginate Aqueous Solutions. *Food Hydrocolloids* **2014**, *38*, 119−128.
(49) Chen, L.; Tian, Y.; Bai, Y.; Wang, J.; Jiao, A.; Jin, Z. Effect of Frying on the Pasting and Rheological Properties of Normal Maize Starch. *Food Hydrocolloids* **2018**, *77*, 85−95.
(50) Franck, A. Creep Recovery Measurements of Polymers 2005 https://www.tainstruments.com/pdf/literature/AAN022_V1b_Creep_Recovery_of_polymer_melts.pdf. (accessed JUne 27, 2025).
(51) Kurek, M.; Benbettaieb, N.; Ščetar, M.; Chaudy, E.; Repajić, M.; Klepac, D.; Valić, S.; Debeaufort, F.; Galić, K. Characterization of Food Packaging Films with Blackcurrant Fruit Waste as a Source of Antioxidant and Color Sensing Intelligent Material. *Molecules* **2021**, *26* (9), No. 2569.
(52) Azmi, N. S.; Basha, R. K.; Othman, S. H.; Mohammed, M. A. P.; Wakisaka, M.; Ariffin, S. H.; Salim, N. H. Development of Fish Gelatin Film for Anti-Fogging Mushroom Packaging. *J. Food Eng.* **2025**, *387*, No. 112306.
(53) Hosseini, S. F.; Rezaei, M.; Zandi, M.; Ghavi, F. F. Preparation and Functional Properties of Fish Gelatin−Chitosan Blend Edible Films. *Food Chem.* **2013**, *136* (3), 1490−1495.
(54) Ibrahim, S. F. B.; Azam, N. A. N. M.; Amin, K. A. M. Sodium Alginate Film: The Effect of Crosslinker on Physical and Mechanical Properties. *IOP Conf. Ser.:Mater. Sci. Eng.* **2019**, *509*, No. 012063, DOI: 10.1088/1757-899X/509/1/012063.
(55) Colinart, T.; Glouannec, P. Accuracy of Water Vapor Permeability of Building Materials Reassessed by Measuring Cup's Inner Relative Humidity. *Build. Environ.* **2022**, *217*, No. 109038.
(56) Zhang, J.; Youngblood, J. P. Cellulose Nanofibril-Based Hybrid Coatings with Enhanced Moisture Barrier Properties. *Mater. Adv.* **2025**, *6* (9), 2833−2844.
(57) Zhao, J.; Song, L.; Ming, W. Antifogging and Frost-Resisting Polymeric Surfaces. In *Advances in Polymer Science*; Springer International Publishing: Cham, 2019; pp 185−214.
(58) Jiang, H.; Zhang, W.; Khan, M. R.; Ahmad, N.; Rhim, J.-W.; Jiang, W.; Roy, S. Film Properties of Pectin Obtained from Various Fruits' (Lemon, Pomelo, Pitaya) Peels. *J. Compos. Sci.* **2023**, *7*, No. 366.
(59) Domínguez-Robles, J.; Larrañeta, E.; Fong, M. L.; Martin, N. K.; Irwin, N. J.; Mutjé, P.; Tarrés, Q.; Delgado-Aguilar, M. Lignin/Poly(Butylene Succinate) Composites with Antioxidant and Antibacterial Properties for Potential Biomedical Applications. *Int. J. Biol. Macromol.* **2020**, *145*, 92−99.
(60) Komitopoulou, E. Microbial and chemical Markers of meat Spoilage. *Int. Meat Top.* **2012**, *3* (3), 23−25.
(61) Xue, H.; Zhao, J.; Wang, Y.; Shi, Z.; Xie, K.; Liao, X.; Tan, J. Factors Affecting the Stability of Anthocyanins and Strategies for Improving Their Stability: A Review. *Food Chem.: X* **2024**, *24*, No. 101883.
(62) Liu, Y.; Tong, Y.; Tong, Q.; Xu, W.; Wang, Z. Effects of Sunflower Pectin on Thermal Stability of Purple Sweet Potato Anthocyanins at Different PH. *Int. J. Biol. Macromol.* **2023**, *253*, No. 126663.
(63) Stintzing, F. C.; Carle, R. Functional Properties of Anthocyanins and Betalains in Plants, Food, and in Human Nutrition. *Trends Food Sci. Technol.* **2004**, *15* (1), 19−38.
(64) Patras, A.; Brunton, N. P.; O'Donnell, C.; Tiwari, B. K. Effect of Thermal Processing on Anthocyanin Stability in Foods; Mechanisms and Kinetics of Degradation. *Trends Food Sci. Technol.* **2010**, *21* (1), 3−11.
(65) Kang, A.; Lee, T. S. Converting Sugars to Biofuels: Ethanol and Beyond. *Bioengineering* **2015**, *2*, 184−203, DOI: 10.3390/bioengineering2040184.
(66) Pramod, C. V.; Fauziah, R.; Seshan, K.; Lange, J.-P. Bio-Based Acrylic Acid from Sugar via Propylene Glycol and Allyl Alcohol. *Catal. Sci. Technol.* **2018**, *8* (1), 289−296.
(67) Polat, Y.; Stojanovska, E.; Negawo, T. A.; Doner, E.; Kilic, A. Lignin as an Additive for Advanced Composites. In *Green Energy and Technology*; Springer International Publishing: Cham, 2017; pp 71−89.
(68) Vavilala, S. L.; Ghag, S. B.; D'Souza, J. S. Lignin: Understanding and Exploring Its Potential for Biofuel Production. In *Advanced Bioprocessing for Alternative Fuels, Biobased Chemicals, and Bioproducts*; Hosseini, M., Ed.; Woodhead Publishing, 2019; Chapter 9, pp 165−186.
(69) Tong, W. Y.; Rafiee, A. R. A.; Leong, C. R.; Tan, W. N.; Dailin, D. J.; Almarhoon, Z. M.; Shelkh, M.; Nawaz, A.; Chuah, L. F. Development of Sodium Alginate-Pectin Biodegradable Active Food Packaging Film Containing Cinnamic Acid. *Chemosphere* **2023**, *336*, No. 139212.
(70) Yüksel, E.; Kort, R.; Voragen, A. G. J. Structure and Degradation Dynamics of Dietary Pectin. *Crit. Rev. Food Sci. Nutr.* **2024**, 1−20, DOI: 10.1080/10408398.2024.2437573.
(71) Chen, L.-Y.; Cheng, C.-W.; Liang, J.-Y. Effect of Esterification Condensation on the Folin−Ciocalteu Method for the Quantitative Measurement of Total Phenols. *Food Chem.* **2015**, *170*, 10−15.
(72) Lee, J.; Durst, R. W.; Wrolstad, R. E.; et al. Determination of Total Monomeric Anthocyanin Pigment Content of Fruit Juices, Beverages, Natural Colorants, and Wines by the PH Differential Method: Collaborative Study. *J. AOAC Int.* **2005**, *88* (5), 1269−1278.

(73) Inácio, M. R. C.; de Lima, K. M. G.; Lopes, V. G.; Pessoa, J. D. C.; de Almeida Teixeira, G. H. Total Anthocyanin Content Determination in Intact Açaí (Euterpe Oleracea Mart.) and Palmitero-Juçara (Euterpe Edulis Mart.) Fruit Using near Infrared Spectroscopy (NIR) and Multivariate Calibration. *Food Chem.* **2013**, *136* (3), 1160−1164.
(74) Do, Q. D.; Angkawijaya, A. E.; Tran-Nguyen, P. L.; Huynh, L. H.; Soetaredjo, F. E.; Ismadji, S.; Ju, Y.-H. Effect of Extraction Solvent on Total Phenol Content, Total Flavonoid Content, and Antioxidant Activity of Limnophila Aromatica. *J. Food Drug Anal.* **2014**, *22* (3), 296−302.
(75) Wexler, A. Vapor Pressure Formulation for Water in Range 0 to 100 Degrees C. A Revision. *J. Res. Natl. Bur. Stand., Sect. A* **1976**, *80A* (5−6), 775−785.
(76) Kanovsky, N.; Margel, S. Fabrication of Transparent Silica/PEG Smooth Thin Coatings on Polymeric Films for Antifogging Applications. *ACS Omega* **2022**, *7* (24), 20505−20514.

https://doi.org/10.1021/acssuschemeng.5c05240
ACS Sustainable Chem. Eng. 2025, 13, 13988−14002